International Journal of Fracture **75:** 19–48, 1996.

Variation of stress intensity factor and crack opening displacement of semi-elliptical surface crack

NAO-AKI NODA and SINSUKE MIYOSHI
Mechanical Engineering Department, Kyushu Institute of Technology, Kitakyushu 804, Japan

Received 5 March 1995; accepted in revised form 30 July 1995

Abstract. In this paper a singular integral equation method is applied to calculate the stress intensity factor along crack front of a 3D surface crack. Stress field induced by body force doublet in a semi infinite body is used as a fundamental solution. Then the problem is formulated as an integral equation with a singularity of the form of r^{-3}. In solving the integral equations, the unknown functions of body force densities are approximated by the product of a polynomial and a fundamental density function; that is, the exact density distribution to make an elliptical crack in an infinite body. The calculation shows that the present method gives the smooth variation of stress intensity factors along the crack front and crack opening displacement along the crack surface for various aspect ratios and Poisson's ratio. The present method gives rapidly converging numerical results and highly satisfactory boundary conditions throughout the crack boundary.

Notation

a	= major radius of a semi-elliptical crack
b	= minor radius of a semi-elliptical crack
(x, y, z)	= rectangular coordinate
(ξ, η, ζ)	= (x, y, z) coordinate where body force is applied
(x', y')	= $(x/a, y/b)$
(ξ', η')	= $(\xi/a, \eta/b)$
E	= Young's modulus
G	= Shear modulus
ν	= Poisson's ratio
H	= $(1-2\nu)/4(1-\nu)^2$
$f(x, y)$	= unknown density function of body force doublet
$w(x, y)$	= fundamental density function of body force
(u_x, u_y, u_z)	= displacement in (x, y, z) direction
$U_z(x', y')$	= crack opening displacement $u_z(x, y, +0) - u_z(x, y, -0)$
$U_{zE}(x', y')$	= crack opening displacement of an elliptical crack
β	= eccentric angle of ellipse
$K_{\mathrm{I}}(\beta)$	= stress intensity factor along the crack front
$K_{\mathrm{I}E}(\beta)$	= stress intensity factor of an elliptical crack
$M_{\mathrm{I}}(\beta)$	= dimensionless stress intensity factor
$F_{\mathrm{I}}(\beta)$	= dimensionless stress intensity factor
$M_{\mathrm{I}}(x', y')$	= dimensionless crack opening displacement

1. Introduction

Problems of surface cracks have attracted the attention of a lot of researchers and engineers because of the importance in design and maintenance of various structures. As a result of computer development, advanced works were carried out by using finite element method [1–10] and other numerical techniques. Nisitani and Murakami [11] first applied the body

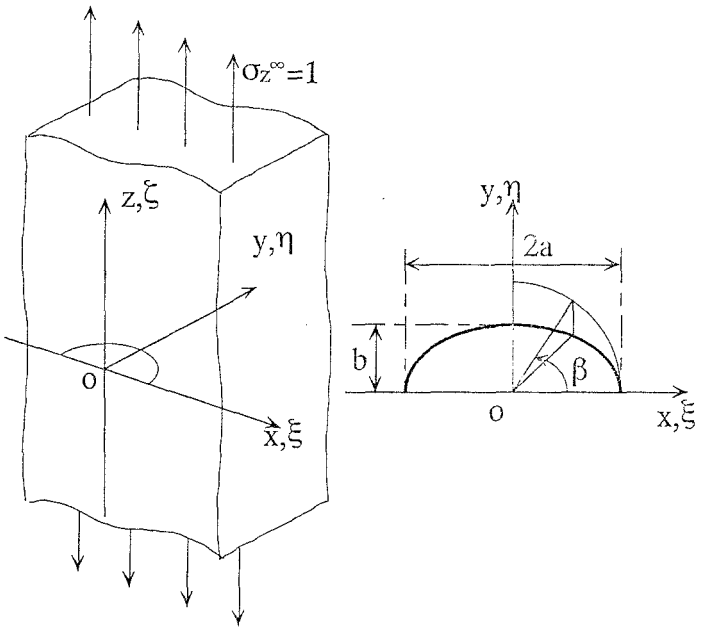

Figure 1. A semi-elliptical crack in a semi-infinite body.

force method to 3D crack problems. Weaver [12], Hayashi–Abe [13], and Takakuda et al. [14] considered the numerical solution of singular integral equations. Murakami–Isida [15] and Isida–Noguchi [16, 17] improved the versatility and accuracy of the body force method. And recently Isida–Tsuru–Noguchi [18, 19] proposed a new method of 3D crack analysis based on the body force method. In spite of the above progress in the analytical aspects, considerable difference is observed among those previous results.

In the previous papers, the numerical solutions of the singular integral equation of the body force method in 2D crack and notch problems have been discussed [20–25]. In those papers unknown functions of the body force densities have been approximated by the products of fundamental density functions and polynomials; it was found that the new method gives results of better accuracy with shorter CPU time compared with the conventional body force method using the step functions [26–28].

In this paper, numerical solution of the singular integral equation in the analysis of 3D crack problems is discussed based on our previous research. To formulate the problem the body force method is applied where the Green's functions for a force doublet is used as the fundamental solution. Then it will be shown that the present method is very useful for analyzing 3D crack problems and giving the smooth variation of stress intensity factor and crack opening displacement with higher accuracy compared with other methods.

2. Numerical solution of singular integral equation

2.1. Singular integral equation of the body force method

Consider a semi-infinite body under uniform tension having a semi-elliptical crack as shown in Figure 1. Here, (ξ, η, ζ) is a (x, y, z) coordinate where body force doublet is applied. Based on the body force method, the problem is reduced to determining the density of force doublet along the prospective boundary of the crack in the semi-infinite body without a crack.

$$\frac{H}{2\pi}\left[\iint\!\!\!\!\!\!\#_S \frac{f(\xi,\eta)}{r_1^3}\,\mathrm{d}\xi\,\mathrm{d}\eta + \iint_S K(\xi,\eta,x,y)f(\xi,\eta)\,\mathrm{d}\xi\,\mathrm{d}\eta\right] = -\sigma_z^{\infty},$$

where

$$K(\xi,\eta,x,y) = -\frac{5-20\nu+24\nu^2}{r_2^3} + \frac{12(1-\nu)(1-2\nu)}{r_2(r_2+y+\eta)^2} + \frac{6\{3y\eta - 2\nu(1-2\nu)(y+\eta)^2\}}{r_2^5}, \tag{1a}$$

$$r_1 = \sqrt{(x-\xi)^2+(y-\eta)^2},$$

$$r_2 = \sqrt{(x-\xi)^2+(y+\eta)^2},$$

$$H = (1-2\nu)/4(1-\nu)^2,$$

$$S = \{(\xi,\eta)|(\xi/a)^2+(\eta/b)^2 \leqslant 1, \eta \geqslant 0\}.$$

The crack opening displacement can be defined by using the body force density $f(x',y')$ as shown in (1b) [20]

$$\left.\begin{aligned} U_z(x',y') &= u_z(x',y',+0) - u_z(x',y',-0) \\ &= \frac{(1-2\nu)(1+\nu)}{E(1-\nu)} f(x',y') \end{aligned}\right\}. \tag{1b}$$

Equation (1) is virtually the boundary condition at the imaginary boundary of a crack; that is, $\sigma_z = 0$. The first term in left-hand side of (1a) expresses the singular term and the notation $\#\!\!\!\!\!\!\#$ should be interpreted as a finite part integral [29]. In the second term $K(\xi,\eta,x,y)$ means the function that satisfies the boundary condition at the free surface.

2.2. Numerical solution of the previous body force method

In the conventional method, the crack region is divided into elements as shown in Figure 2 and the unknown function of the body force densities has been approximated by the product of the fundamental density functions and the stepped functions as shown in the following expression

$$\left.\begin{aligned} &f^{(j)}(\xi,\eta) = f_j \cdot w(\xi,\eta), \\ &\text{where} \\ &w(\xi,\eta) = \frac{b\sigma_z^{\infty}}{H\Phi}\sqrt{1-(\xi/a)^2-(\eta/b)^2} \end{aligned}\right\}, \tag{2a}$$

$$\Phi = \left\{\begin{aligned} &E(k), \quad k = \sqrt{1-(b/a)^2} \quad (a \geqslant b) \\ &\frac{b}{a}E(k'), \quad k' = \sqrt{1-(a/b)^2} \quad (a < b) \end{aligned}\right\}. \tag{2b}$$

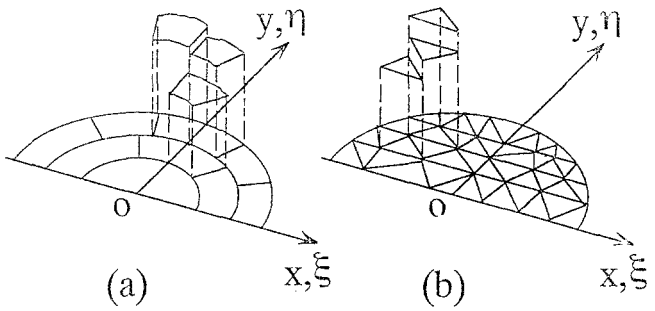

Figure 2. Approximation of weighting function using the step function at each element. (a) Nisitani–Murakami [11], Murakami–Isida [16–17] (b) Murakami–Isida [15].

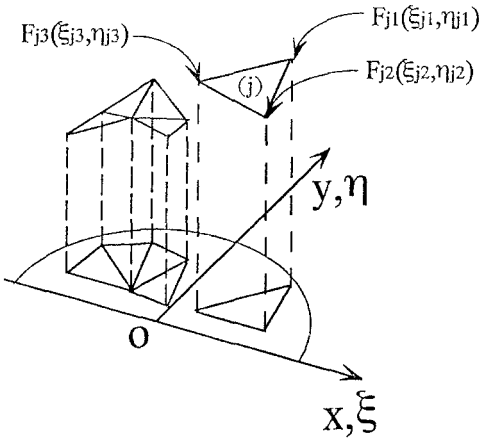

Figure 3. Approximation of weighting function using the linear function at each element (Isida–Tsuru–Noguchi [18, 19]).

Here, $w(x, y)$ is a fundamental density function of a body force, which expresses the stress field due to an elliptical crack in an infinite body and leads to solutions with high accuracy. Here, the weight function f_j is assumed as a stepped function having constant value at jth element as shown in (2) [11, 15–17]. However, the step function expressions of the body force densities give rise to singularities along the element boundaries, and they tend to deteriorate the accuracy and validity in sophisticated problems. Isida et al. [18, 19] have therefore proposed the method of approximation expressed by the following equation

$$f^{(j)}(\xi, \eta) = F_j(\xi, \eta) w(\xi, \eta), \tag{3}$$

where $F_j(\xi, \eta)$ is a linear function of the coordinate as shown in Figure 3.

$$F_j(\xi, \eta) = c_j \xi + d_j \eta + e_j. \tag{4}$$

2.3. Numerical solution of the present method

In the present analysis, polynomials have been used to approximate the unknown functions as a continuous function. First, we put

$$\left.\begin{aligned} &f(\xi,\eta) = F(\xi',\eta')w(\xi',\eta'),\\ &\text{where}\\ &w(\xi',\eta') = \frac{b\sigma_z^{\infty}}{H\Phi}\sqrt{1-\xi'^2-\eta'^2}, \quad \xi' = \xi/a, \quad \eta' = \eta/b \end{aligned}\right\}. \tag{5}$$

Then, the integral equation (1) becomes

$$\left.\begin{aligned} &\frac{b}{2\pi\Phi}\left[\#\!\!\!\!\!\!\int\!\!\!\!\!\!\int_S \frac{F(\xi',\eta')}{r_1^3}\sqrt{1-\xi'^2-\eta'^2}\,\mathrm{d}\xi\,\mathrm{d}\eta\right.\\ &\left.+\int\!\!\int_S K(\xi,\eta,x,y)F(\xi',\eta')\sqrt{1-\xi'^2-\eta'^2}\,\mathrm{d}\xi\,\mathrm{d}\eta\right] = -1 \end{aligned}\right\}. \tag{6}$$

Here, $F(\xi',\eta')$ is now approximated in terms of polynomials as follows

$$\left.\begin{aligned} F(\xi',\eta') = {} & \alpha_0 + \alpha_1\eta' + \cdots \alpha_{n-1}\eta'^{n-1} + \alpha_n\eta'^{n}\\ & + \alpha_{n+1}\xi'^{2\times 1} + \alpha_{n+2}\xi'^{2\times 1}\eta' + \cdots + \alpha_{2n}\xi'^{2\times 1}\eta'^{n-1}\\ & \vdots \qquad\qquad \vdots\\ & + \alpha_{l-2}\xi'^{2\cdot(n-1)} + \alpha_{l-1}\xi'^{2\cdot(n-1)}\eta'\\ & + \alpha_l\xi'^{2\cdot n}\\ = {} & \sum_{i=0}^{l}\alpha_i G_i(\xi',\eta'), \end{aligned}\right\}. \tag{7}$$

where

$$\left.\begin{aligned} l = {} & \sum_{k=0}^{n}(k+1)\\ = {} & \frac{(n+1)(n+2)}{2},\\ G_0(\xi',\eta') = {} & 1, G_1(\xi',\eta') = \eta', \ldots\\ & \ldots, G_{n+1}(\xi',\eta') = \xi'^{2\times 1}, \ldots, G_l(\xi',\eta') = \xi'^{2\cdot n} \end{aligned}\right\}$$

Using the approximation method mentioned above, we obtain the following system of linear equations for the determination of the coefficients α_i. The unknown coefficients $\alpha_i\,[i = 0,1,2,\ldots l, l = (1/2)(n+1)(n+2)]$ are then determined from (8) by selecting a set of collocation points.

$$\left.\begin{aligned} &\frac{b}{2\pi\Phi}\sum_{i=0}^{l}\alpha_i(A_i+B_i)=-1, \\ &\text{where} \\ &A_i=\iint_S \frac{G_i(\xi',\eta')}{r_1^3}\sqrt{1-\xi'^2-\eta'^2}\,\mathrm{d}\xi\,\mathrm{d}\eta, \\ &B_i=\int\!\!\int_S K(\xi,\eta,x,y)G_i(\xi',\eta')\sqrt{1-\xi'^2-\eta'^2}\,\mathrm{d}\xi\,\mathrm{d}\eta \end{aligned}\right\}. \tag{8}$$

3. Numerical evaluation of hypersingular integrals

In (8) the integral B_i can be evaluated numerically because of no singularities in the integral. However, A_i cannot be evaluated by ordinary numerical procedures because they have hypersingularities of the form r^{-3} when $x=\xi$ and $y=\eta$; therefore, the following method is applied. First, we put

$$\left.\begin{aligned} A_i &= \iint_{S+S_c} \frac{G_i(\xi',\eta')}{r_1^3}\sqrt{1-\xi'^2-\eta'^2}\,\mathrm{d}\xi\,\mathrm{d}\eta \\ &\quad -\int\!\!\int_{S_c} \frac{G_i(\xi',\eta')}{r_1^3}\sqrt{1-\xi'^2-\eta'^2}\,\mathrm{d}\xi\,\mathrm{d}\eta \\ &= A_{1i}-A_{2i}, \\ &\text{where} \\ &S+S_c=\{(\xi',\eta')|\xi'^2+\eta'^2\leqslant 1\}, \\ &S_c=\{(\xi',\eta')|\xi'^2+\eta'^2\leqslant 1,\eta'\leqslant 0\} \end{aligned}\right\}. \tag{9}$$

The regions of integral S and S_c are shown in Figure 4. The integral A_{2i} can be evaluated easily because of no singularities. Next, in order to evaluate the integral A_{2i} the following expressions will be used

$$\begin{aligned} &\xi'=\xi/a,\quad \eta'=\eta/b,\quad x'=x/a,\quad y'=y/b, \\ &\sqrt{1-\xi'^2-\eta'^2}=\sqrt{1-x'^2-y'^2} \\ &\qquad -\frac{x'}{\sqrt{1-x'^2-y'^2}}(\xi'-x')-\frac{y'}{\sqrt{1-x'^2-y'^2}}(\eta'-y') \\ &\qquad -\frac{1}{\sqrt{1-x'^2-y'^2}(\sqrt{1-\xi'^2-\eta'^2}+\sqrt{1-x'^2-y'^2})} \\ &\qquad \times\left[\frac{(1-y'^2)(\xi'+x')}{(x'\sqrt{1-\xi'^2-\eta'^2}+\xi'\sqrt{1-x'^2-y'^2})}\cdot(\xi'-x')^2\right. \\ &\qquad +\left\{\frac{x'^2(\eta'+y')}{(x'\sqrt{1-\xi'^2-\eta'^2}+\xi'\sqrt{1-x'^2-y'^2})}\right. \end{aligned}$$

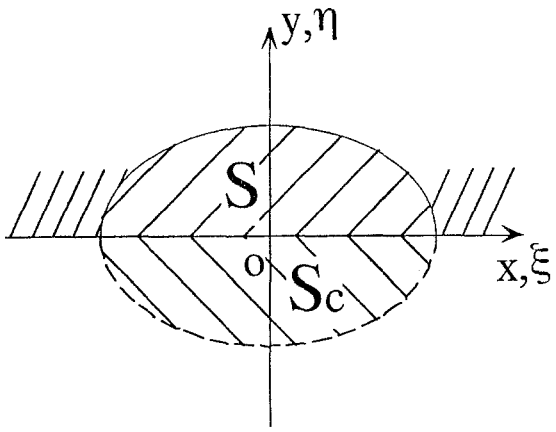

Figure 4. Domain of integral.

$$+\frac{y'^2(\xi'+x')}{(y'\sqrt{1-\xi'^2-\eta'^2}+\eta'\sqrt{1-x'^2-y'^2})}\Bigg\}(\xi'-x')(\eta'-y') \tag{10}$$

$$+\frac{(1-x'^2)(\eta'+y')}{(y'\sqrt{1-\xi'^2-\eta'^2}+\eta'\sqrt{1-x'^2-y'^2})}\cdot(\eta'-y')^2\Bigg]$$

$$\begin{aligned}
&= S_{00}(x',y') + S_{10}(x',y')\cdot(\xi'-x') + S_{11}(x',y')\cdot(\eta'-y') \\
&\quad + S_{20}(\xi',\eta',x',y')\cdot(\xi'-x')^2 \\
&\quad + S_{21}(\xi',\eta',x',y')\cdot(\xi'-x')(\eta'-y') \\
&\quad + S_{22}(\xi',\eta',x',y')\cdot(\eta'-y')^2,
\end{aligned}$$

$$\begin{aligned}
\xi'^{2n} &= x'^{2n} + 2nx'^{2n-1}\cdot(\xi'-x') + \sum_{i=0}^{2n-2}\{(i+1)\cdot\xi^{(2n-2-i)}\cdot x^i\}\cdot(\xi'-x')^2 \\
&= b_0(x') + b_1(x')\cdot(\xi'-x') + b_2(\xi',x')\cdot(\xi'-x')^2, \\
\eta'^n &= y'^n + ny'^{n-1}\cdot(\eta'-y') + \sum_{i=0}^{n-2}\{(i+1)\cdot\eta^{(n-2-i)}\cdot y^i\}\cdot(\eta'-y')^2 \\
&= c_0(y') + c_1(y')\cdot(\eta'-y') + c_2(\eta',y')\cdot(\eta'-y')^2.
\end{aligned}$$

In (10), it should be noted that $S_{00}(x',y'), S_{10}(x',y'), S_{11}(x',y'), b_0(x'), b_1(x'), c_0(y')$, $c_1(y')$ are independent of ξ, η. By using a polar coordinate shown in Figure 5, (10) becomes

$$\begin{aligned}
\sqrt{1-\xi'^2-\eta'^2} &= A_0 + A_1(\theta)\cdot r + A_2(r,\theta)\cdot r^2, \\
\xi'^{2n} &= B_{0i} + B_{1i}(\theta)\cdot r + B_{2i}(r,\theta)\cdot r^2, \\
\eta'^n &= C_{0i} + C_{1i}(\theta)\cdot r + C_{2i}(r,\theta)\cdot r^2,
\end{aligned}$$

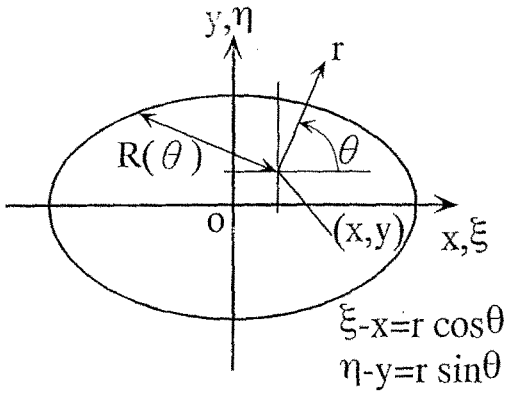

Figure 5. Change of integral parameter from (ξ, η) to (r, θ).

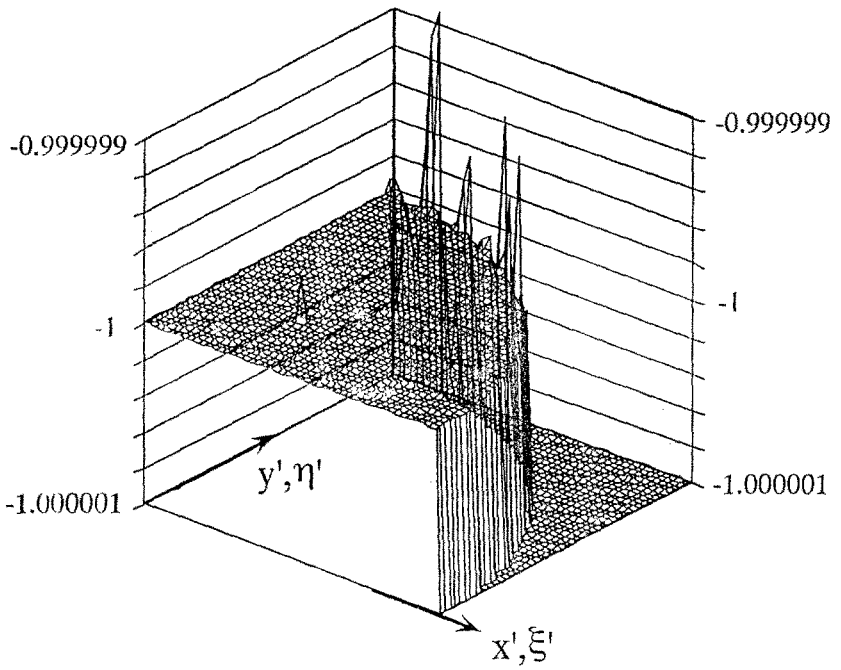

Figure 6. Numerical value of integral $(b/a = 1)$.

where

$$
\begin{aligned}
A_0 &= S_{00}(x', y'), \\
A_1(\theta) &= S_{10}(x', y') \cdot \cos\theta + S_{11}(x', y') \cdot \sin\theta, \\
A_2(r, \theta) &= S_{20}(\xi', \eta', x', y') \cdot \cos^2\theta \\
&\quad + S_{21}(\xi', \eta', x', y') \cdot \cos\theta \cdot \sin\theta \\
&\quad + S_{22}(\xi', \eta', x', y') \cdot \sin^2\theta,
\end{aligned}
\tag{11}
$$

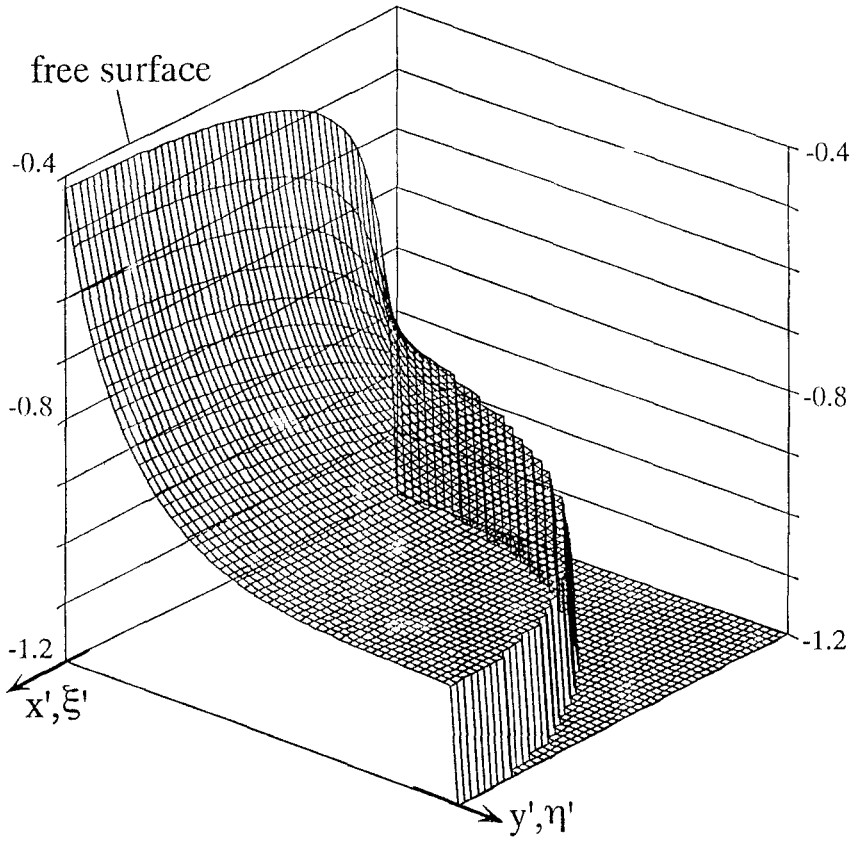

$$\frac{b}{2\pi\Phi}\{A_i + B_i\} \quad , \quad G_i(\xi', \eta') = 1$$

Figure 7. Numerical value of integral ($b/a = 1, \nu = 0.3$).

$$\begin{aligned} B_0 &= b_0(x'), \\ B_1(\theta) &= b_1(x') \cdot \cos\theta, \\ B_2(r,\theta) &= b_2(\xi', x') \cdot \cos^2\theta, \end{aligned}$$

$$\begin{aligned} C_0 &= c_0(y'), \\ C_1(\theta) &= c_1(y') \cdot \sin\theta, \\ C_2(r,\theta) &= c_2(\eta', y') \cdot \sin^2\theta. \end{aligned}$$

Then, we can also obtain the expression

$$G_i(\xi', \eta')\sqrt{1 - \xi'^2 - \eta'^2} = D_{0i} + D_{1i}(\theta) \cdot r + D_{2i}(r,\theta) \cdot r^2,$$

where

$$\begin{aligned} D_{0i} &= A_0 \cdot B_0 \cdot C_0, \\ D_{1i}(\theta) &= A_0 \cdot B_0 \cdot C_1 + A_0 \cdot B_1 \cdot C_0 + A_1 \cdot B_0 \cdot C_0, \end{aligned}$$

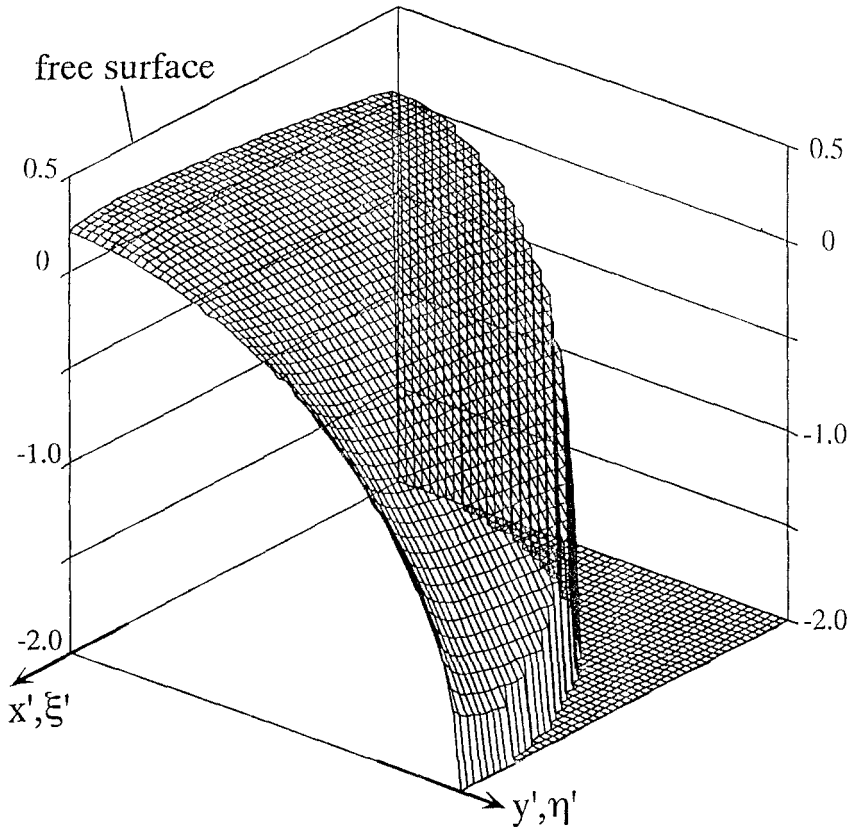

$$\frac{b}{2\pi\Phi}\{A_i + B_i\} \quad , \quad G_i(\xi', \eta') = \xi'^2$$

Figure 8. Numerical value of integral ($b/a = 1, \nu = 0.3$).

$$\begin{aligned} D_{2i}(r,\theta) = {} & A_0 \cdot B_0 \cdot C_2 + A_0 \cdot B_2 \cdot C_0 + A_2 \cdot B_0 \cdot C_0 + A_0 \cdot B_1 \cdot C_1 + A_1 \cdot B_0 \cdot C_1 \\ & + A_1 \cdot B_1 \cdot C_0 + A_0 \cdot B_1 \cdot C_2 + A_1 \cdot B_0 \cdot C_2 + A_0 \cdot B_2 \cdot C_1 \\ & + A_1 \cdot B_2 \cdot C_0 + A_2 \cdot B_0 \cdot C_1 + A_2 \cdot B_1 \cdot C_0 + A_1 \cdot B_1 \cdot C_1 \\ & + A_0 \cdot B_2 \cdot C_2 + A_1 \cdot B_1 \cdot C_2 + A_2 \cdot B_0 \cdot C_2 + A_1 \cdot B_2 \cdot C_1 \\ & + A_2 \cdot B_2 \cdot C_0 + A_2 \cdot B_1 \cdot C_1 + A_1 \cdot B_2 \cdot C_2 + A_2 \cdot B_1 \cdot C_2 \\ & + A_2 \cdot B_2 \cdot C_1 + A_2 \cdot B_2 \cdot C_2. \end{aligned} \tag{12}$$

By substituting (12) into (9) we obtain

$$\begin{aligned} A_{1i} = {} & \int_0^{2\pi} \fint_0^{R(\theta)} \left[\frac{D_{0i}}{r^2} + \frac{D_{1i}(\theta)}{r}\right] \mathrm{d}r\, \mathrm{d}\theta \\ & + \int_0^{2\pi} \int_0^{R(\theta)} [D_{2i}(r,\theta)]\, \mathrm{d}r\, \mathrm{d}\theta \\ = {} & A_{ai} + A_{bi}, \end{aligned} \tag{13}$$

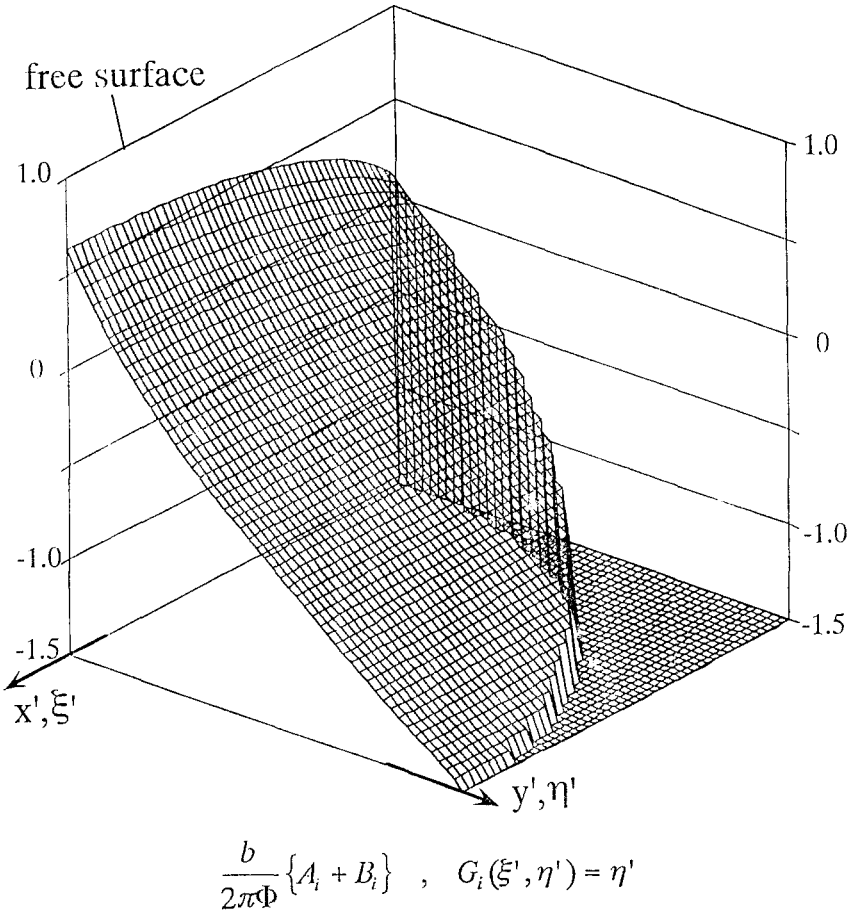

Figure 9. Numerical value of integral ($b/a = 1, \nu = 0.3$).

where

$$R(\theta) = \frac{\{-((x \cdot \cos\theta/a^2) + (y \cdot \sin\theta/b^2))}{(\cos\theta/a)^2 + (\sin\theta/b)^2}$$
$$\frac{}{+\sqrt{(\cos\theta/a)^2 + (\sin\theta/b)^2 - [(x \cdot \sin\theta - y \cdot \cos\theta)/(a \cdot b)]^2}\}}.$$

Here, A_{bi} has no singularities and can be evaluated easily in numerical integration. On the other hand, A_{bi} has singularities; however, they are expressed simply in the form r^{-1} or r^{-2}, so they can be evaluated in the Hadamard sense as shown in (10).

$$A_{ai} = \int_0^{2\pi} \left[-\frac{D_{0i}}{R(\theta)} + D_{1i}(\theta) \cdot \log(R(\theta)) \right] d\theta. \tag{14}$$

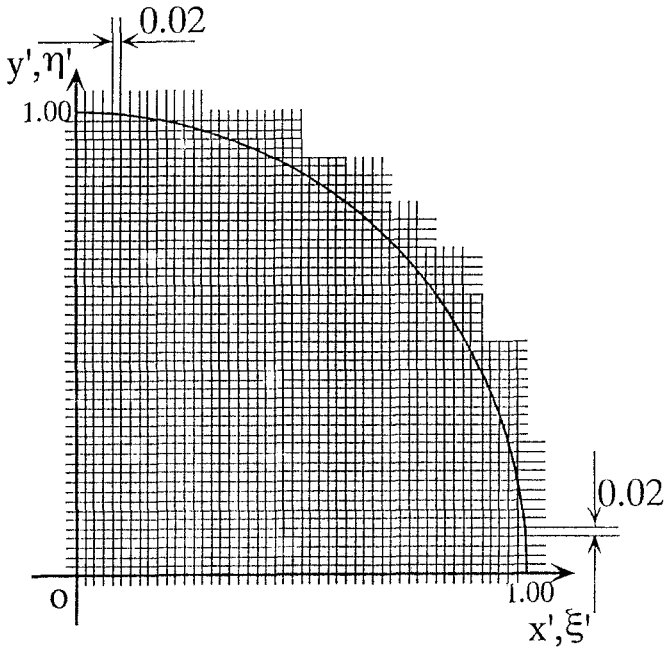

Figure 10. Boundary collocation points.

4. Numerical results and discussion

4.1. Representation of the numerical results

Numerical calculations have been carried out for changing n in (7). Numerical integrals have been performed using scientific subroutine library (FACOM SSL II DAQE etc.). In demonstrating the numerical results of stress intensity factor (SIF) $K_{\mathrm{I}}(\beta)$ and crack opening displacement (COD) $U_z(x', y')$, the following three kinds of dimensionless factors $M_{\mathrm{I}}(\beta)$, $F_{\mathrm{I}}(\beta)$ for SIF, and $M_{\mathrm{I}}(x', y')$ for COD, will be used

$$M_{\mathrm{I}} = \frac{K_{\mathrm{I}}(\beta)}{K_{\mathrm{I}E}(\beta)} = F(\xi', \eta')|_{\xi'=\cos\beta, \eta'=\sin\beta},$$

where

$$K_{\mathrm{I}E}(\beta) = \frac{\sigma_z^{\infty}\sqrt{\pi b}}{\Phi}\left[\sin^2\beta + \left(\frac{b}{a}\right)^2\cos^2\beta\right]^{1/4},$$

$$F_{\mathrm{I}} = \frac{K_{\mathrm{I}}(\beta)}{\sigma_z^{\infty}\sqrt{\pi b}} = \frac{F(\xi', \eta')|_{\xi'=\cos\beta, \eta'=\sin\beta}}{\Phi}\left[\sin^2\beta + \left(\frac{b}{a}\right)^2\cos^2\beta\right]^{1/4}, \tag{15}$$

$$M_{\mathrm{I}}(x', y') = \frac{U_z(x', y')}{U_{zE}(x', y')} = F(x', y'),$$

where

$$U_{zE}(x', y') = \frac{4(1-\nu^2)}{E}\frac{b\sigma_z^{\infty}}{\Phi}\sqrt{1 - x'^2 - y'^2}.$$

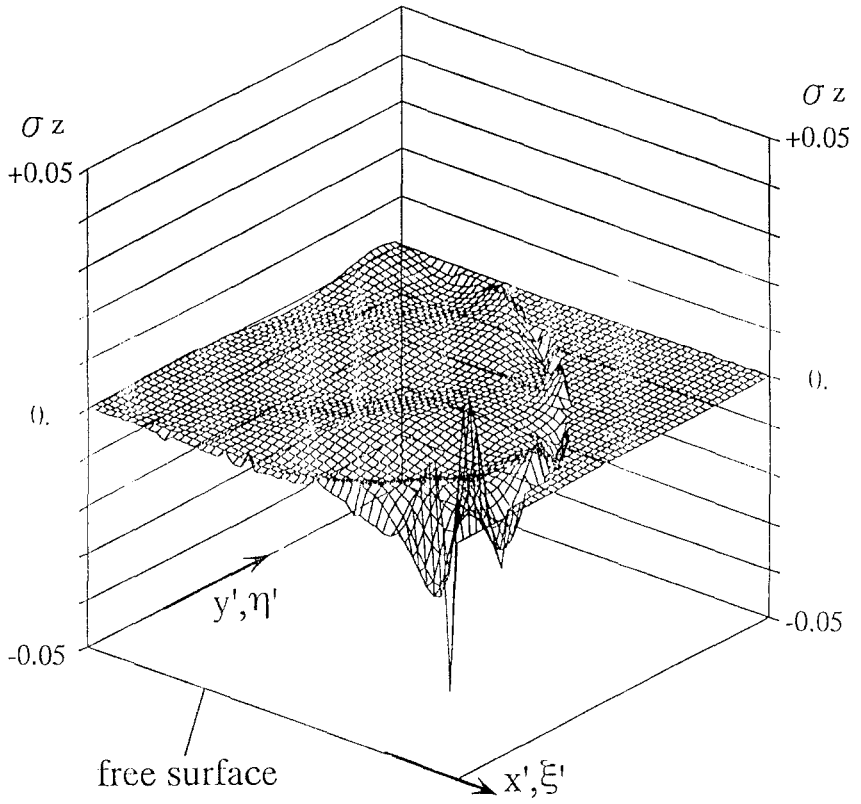

$$\sigma_z = \frac{b}{2\pi\Phi}\sum_{i=0}^{l}\alpha_i\left(A_i + B_i\right) + 1$$

Figure 11. Compliance of boundary condition ($n = 8, \nu = 0.3, b/a = 1$).

Here, $M_{\mathrm{I}}(\beta)$ is defined as the multiple of the stress intensity factor of the elliptical crack with principal diameters $2a$ and $2b$ embedded in an infinite solid $K_{\mathrm{I}}(\beta)$, and is relevant to comparing the present results with previous ones. The other factor $F_{\mathrm{I}}(\beta)$, on the other hand, is expressed on the basis of the stress intensity factor of the plane strain internal crack of length $2b$, and is suitable for comparing the magnitudes of the stress intensity factors at different points on the crack front or the maximum one of differently shaped cracks. Also, $M_{\mathrm{I}}(\xi', \eta')$ is defined as the multiple of the crack opening displacement of the elliptical crack with principal diameters $2a$ and $2b$ embedded in an infinite solid $U_{zE}(\xi', \eta')$.

4.2. Convergency of numerical results

In this analysis it is important to evaluate the numerical integrals accurately. As an example, Figure 6 shows the value of integral A_{1i} in (9) when $G_i(\xi', \eta') = 1$, which is corresponding to the stress σ_z along the embedded elliptical crack in an infinite body expressed by the distribution of the exact body force density $w(\xi, \eta)$. As shown in Figure 6, the stress coincides with the exact value $\sigma_z = -1$ by 10 significant digits for most cases, and by 6 digits for the

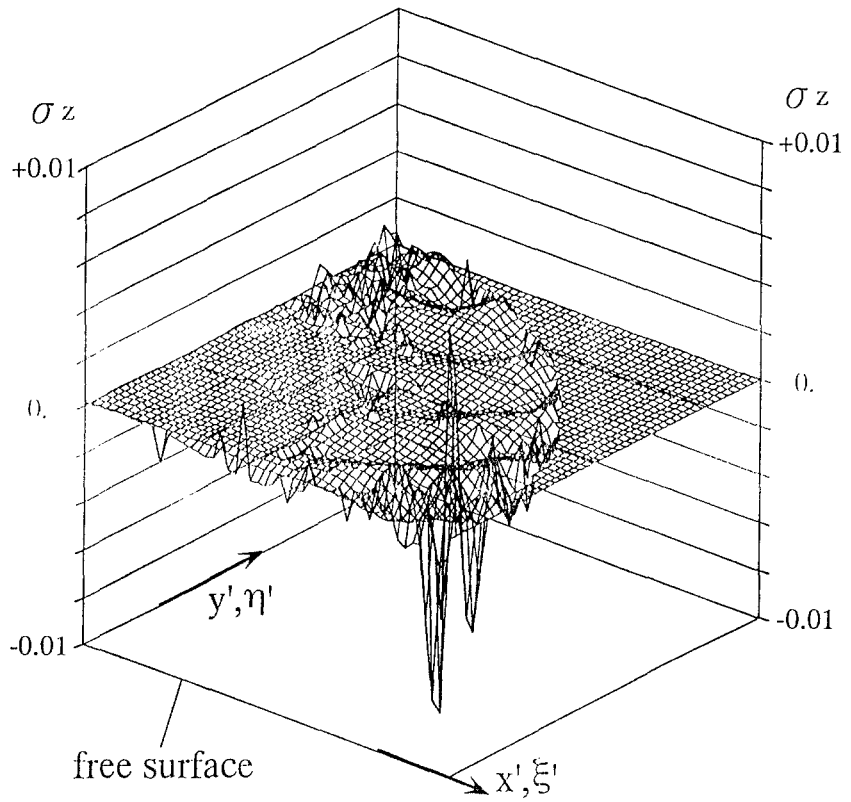

$$\sigma_z = \frac{b}{2\pi\Phi}\sum_{i=0}^{l}\alpha_i\left(A_i + B_i\right) + 1$$

Figure 12. Compliance of boundary condition ($n = 13, \nu = 0.3, b/a = 1$).

worst cases near the crack front. This indicates the validity of calculation of hypersingular integral and the high accuracy of the numerical integral procedure.

Figures 7–9 show the values of integrals $(A_i + B_i)b/(2\pi\Phi)$ in (8) when $G_i(\xi', \eta') = 1, G_i(\xi', \eta') = \xi'^2, G_i(\xi', \eta') = \eta'$ for $b/a = 1$ and $\nu = 0.3$. In this analysis the boundary condition for crack surface $\sigma_z = -1$ will be satisfied by superposing the smooth functions as indicated in Figures 7–9. Here, the boundary conditions are considered at the intersection of the mesh whose interval is 0.02 as shown in Figure 10. On the line $y' = 0$ the integral B_i in (8) and A_{2i} in (9) cannot be calculated; then, the boundary conditions are considered on the line $y' = 0.015$ instead of $y' = 0$. In solving the algebraic equation (6) the least square regression method is applied to minimize the residual of stresses at the collocation points.

Figures 11–16 indicate the compliance of the boundary conditions along the prospective crack surface with varying n in (7). The boundary condition becomes highly satisfied with increasing n and when $\nu = 0.3$ and $n = 18$ the error is less than 3×10^{-3} throughout the range $\eta' \geqslant 0.015$. The boundary condition is especially highly satisfied when $\nu = 0$ within the error 1×10^{-3}.

Table 1. Convergency of dimensionless stress intensity factors $F_I(\nu = 0, b/a = 1)$

β (deg) / n	0	1	2	3	4	5	6	7	8	9	10	15	20	25
11	0.76598	0.75104	0.73871	0.72847	0.71990	0.71264	0.70642	0.70101	0.69623	0.69196	0.68811	0.67321	0.66321	0.65622
12	0.76660	0.75116	0.73862	0.72833	0.71979	0.71258	0.70641	0.70102	0.69625	0.69197	0.68811	0.67319	0.66324	0.65620
13	0.76716	0.75130	0.73858	0.72826	0.71975	0.71258	0.70642	0.70104	0.69626	0.69197	0.68809	0.67319	0.66325	0.65618
14	0.76770	0.75145	0.73859	0.72825	0.71974	0.71260	0.70646	0.70108	0.69629	0.69199	0.68810	0.67319	0.66325	0.65618
15	0.76801	0.75150	0.73855	0.72820	0.71972	0.71259	0.70646	0.70108	0.69629	0.69198	0.68808	0.67320	0.66324	0.65619
16	0.76815	0.75141	0.73841	0.72808	0.71964	0.71255	0.70644	0.70107	0.69629	0.69198	0.68809	0.67320	0.66324	0.65620
17	0.76838	0.75147	0.73841	0.72806	0.71962	0.71254	0.70643	0.70107	0.69628	0.69198	0.68809	0.67321	0.66323	0.65620
18	0.76865	0.75154	0.73842	0.72807	0.71965	0.71258	0.70646	0.70109	0.69629	0.69198	0.68809	0.67321	0.66323	0.65621
19	0.76874	0.75152	0.73838	0.72806	0.71966	0.71260	0.70650	0.70111	0.69632	0.69200	0.68811	0.67321	0.66324	0.65622
20	0.76882	0.75154	0.73840	0.72807	0.71967	0.71261	0.70650	0.70112	0.69632	0.69200	0.68811	0.67321	0.66324	0.65622

β (deg) / n	30	35	40	45	50	55	60	65	70	75	80	85	90
11	0.65103	0.64716	0.64426	0.64196	0.64049	0.63881	0.63777	0.63690	0.63625	0.63583	0.63554	0.63530	0.63519
12	0.65102	0.64719	0.64424	0.64194	0.64020	0.63883	0.63772	0.63693	0.63629	0.63582	0.63548	0.63533	0.63531
13	0.65103	0.64718	0.64422	0.64196	0.64020	0.63880	0.63774	0.63692	0.63627	0.63581	0.63550	0.63531	0.63521
14	0.65105	0.64717	0.64422	0.64197	0.64019	0.63881	0.63775	0.63690	0.63627	0.63582	0.63549	0.63532	0.63524
15	0.65105	0.64716	0.64423	0.64196	0.64019	0.63882	0.63774	0.63690	0.63628	0.63581	0.63550	0.63531	0.63524
16	0.65104	0.64717	0.64424	0.64195	0.64019	0.63881	0.63773	0.63691	0.63628	0.63581	0.63550	0.63531	0.63523
17	0.65104	0.64718	0.64424	0.64195	0.64019	0.63881	0.63774	0.63691	0.63627	0.63581	0.63550	0.63531	0.63523
18	0.65103	0.64718	0.64424	0.64196	0.64019	0.63881	0.63774	0.63691	0.63628	0.63581	0.63549	0.63530	0.63524
19	0.65103	0.64718	0.64423	0.64196	0.64019	0.63881	0.63774	0.63691	0.63628	0.63581	0.63549	0.63529	0.63522
20	0.65103	0.64718	0.64423	0.64196	0.64019	0.63881	0.63774	0.63691	0.63628	0.63581	0.63549	0.63529	0.63522

Table 2. Convergency of dimensionless stress intensity factors $F_{\mathrm{I}}(\nu = 0, b/a = 0.25)$

β (deg) / n	0	1	2	3	4	5	6	7	8	9	10	15	20	25
11	0.66908	0.64574	0.62811	0.61535	0.60717	0.60150	0.59909	0.59895	0.60061	0.60368	0.60783	0.63839	0.67638	0.71658
12	0.67114	0.64648	0.62817	0.61514	0.60647	0.60134	0.59904	0.59899	0.60068	0.60375	0.60787	0.63807	0.67637	0.71666
13	0.67279	0.64697	0.62807	0.61483	0.60614	0.60107	0.59886	0.59885	0.60056	0.60360	0.60766	0.63777	0.67635	0.71658
14	0.67415	0.64734	0.62800	0.61465	0.60600	0.60105	0.59892	0.59895	0.60066	0.60365	0.60765	0.63767	0.67645	0.71658
15	0.67508	0.64755	0.62795	0.61457	0.60600	0.60112	0.59905	0.59910	0.60079	0.60375	0.60773	0.63780	0.67645	0.71646
16	0.67588	0.64783	0.62804	0.61462	0.60606	0.60120	0.59911	0.59915	0.60080	0.60374	0.60771	0.63782	0.67645	0.71649
17	0.67659	0.64790	0.62788	0.61443	0.60599	0.60113	0.59909	0.59914	0.60079	0.60372	0.60768	0.63789	0.67643	0.71651
18	0.67733	0.64817	0.62796	0.61448	0.60601	0.60123	0.59919	0.59923	0.60085	0.60375	0.60770	0.63789	0.67641	0.71655
19	0.67788	0.64833	0.62797	0.61446	0.60599	0.60122	0.59917	0.59918	0.60078	0.60368	0.60763	0.63790	0.67638	0.71656
20	0.67781	0.64827	0.62786	0.61440	0.60598	0.60123	0.59920	0.59920	0.60079	0.60368	0.60762	0.63787	0.67637	0.71660

β (deg) / n	30	35	40	45	50	55	60	65	70	75	80	85	90
11	0.75549	0.79184	0.82567	0.85645	0.88380	0.90806	0.92925	0.94701	0.96144	0.97285	0.98104	0.98573	0.98719
12	0.75539	0.79189	0.82573	0.85629	0.88376	0.90817	0.92916	0.94690	0.96159	0.97290	0.98085	0.98582	0.98762
13	0.75528	0.79192	0.82566	0.85624	0.88384	0.90813	0.92912	0.94703	0.96156	0.97279	0.98098	0.98584	0.98738
14	0.75532	0.79192	0.82560	0.85630	0.88384	0.90810	0.92920	0.94698	0.96153	0.97291	0.98092	0.98582	0.98755
15	0.75532	0.79190	0.82563	0.85633	0.88381	0.90814	0.92917	0.94696	0.96158	0.97285	0.98091	0.98583	0.98748
16	0.75534	0.79187	0.82565	0.85632	0.88382	0.90814	0.92916	0.94698	0.96157	0.97284	0.98091	0.98581	0.98745
17	0.75537	0.79186	0.82566	0.85632	0.88383	0.90812	0.92916	0.94699	0.96155	0.97285	0.98089	0.98578	0.98745
18	0.75537	0.79186	0.82567	0.85631	0.88383	0.90812	0.92917	0.64697	0.96155	0.97285	0.98089	0.98578	0.98744
19	0.75534	0.79185	0.82565	0.85631	0.88382	0.90811	0.92916	0.94695	0.96156	0.97284	0.98089	0.98580	0.98744
20	0.75532	0.79186	0.82564	0.85630	0.88381	0.90812	0.92915	0.94695	0.96156	0.97284	0.98089	0.98579	0.98743

Table 3. Convergency of dimensionless stress intensity factors $F_I(\nu = 0.3, b/a = 1)$

β (deg) / n	1	2	3	4	5	6	7	8	9	10	15	20	25
11	0.7436	0.7424	0.7414	0.7400	0.7381	0.7355	0.7324	0.7288	0.7252	0.7216	0.70699	0.69722	0.68851
12	0.7431	0.7431	0.7427	0.7415	0.7393	0.7362	0.7337	0.7288	0.7250	0.7213	0.70739	0.69716	0.68837
13	0.7411	0.7428	0.7433	0.7423	0.7400	0.7367	0.7329	0.7288	0.7250	0.7213	0.70764	0.69709	0.68846
14	0.7408	0.7438	0.7447	0.7437	0.7411	0.7375	0.7334	0.7292	0.7252	0.7215	0.70777	0.69689	0.68860
15	0.7401	0.7441	0.7453	0.7441	0.7413	0.7375	0.7333	0.7292	0.7252	0.7217	0.70782	0.69678	0.68873
16	0.7417	0.7462	0.7473	0.7457	0.7424	0.7382	0.7337	0.7293	0.7253	0.7217	0.70781	0.69684	0.68881
17	0.7416	0.7467	0.7480	0.7464	0.7430	0.7386	0.7339	0.7294	0.7254	0.7218	0.70782	0.69692	0.68891
18	0.7413	0.7465	0.7477	0.7459	0.7423	0.7379	0.7334	0.7291	0.7252	0.7217	0.70776	0.69696	0.68892
19	0.7418	0.7459	0.7478	0.7456	0.7419	0.7376	0.7333	0.7292	0.7247	0.7214	0.70761	0.69710	0.68890
20	0.7422	0.7456	0.7476	0.7455	0.7410	0.7367	0.7326	0.7287	0.7243	0.7213	0.70758	0.69712	0.68883
β (deg) / n	30	35	40	45	50	55	60	65	70	75	80	85	90
11	0.68195	0.67738	0.67300	0.66924	0.66681	0.66472	0.66255	0.66109	0.66029	0.65939	0.65858	0.65840	0.65850
12	0.68224	0.67712	0.67267	0.66954	0.66686	0.66436	0.66270	0.66144	0.66007	0.65918	0.65882	0.65838	0.65808
13	0.68231	0.67697	0.67277	0.66960	0.66670	0.66447	0.66278	0.66121	0.66016	0.65939	0.65865	0.65852	0.65871
14	0.68230	0.67691	0.67288	0.66950	0.66671	0.66457	0.66267	0.66128	0.66020	0.65923	0.65871	0.65828	0.65797
15	0.68223	0.67703	0.67294	0.66947	0.66677	0.66448	0.66268	0.66127	0.66012	0.65937	0.65872	0.65845	0.65852
16	0.68221	0.67706	0.67294	0.66948	0.66675	0.66453	0.66272	0.66124	0.66016	0.65935	0.65875	0.65850	0.65846
17	0.68219	0.67711	0.67291	0.66950	0.66676	0.66455	0.66274	0.66123	0.66020	0.65934	0.65871	0.65824	0.65797
18	0.68219	0.67710	0.67291	0.66949	0.66677	0.66455	0.66272	0.66126	0.66016	0.65929	0.65868	0.65827	0.65811
19	0.68216	0.67708	0.67287	0.66950	0.66674	0.66456	0.66270	0.66130	0.66014	0.65928	0.65871	0.65834	0.65847
20	0.68211	0.67708	0.67287	0.66950	0.66674	0.66455	0.66271	0.66128	0.66014	0.65930	0.65873	0.65834	0.65849

Table 4. Convergency of dimensionless stress intensity factors $F_I(\nu = 0.3, b/a = 0.25)$

β (deg) / n	1	2	3	4	5	6	7	8	9	10	15	20	25
11	0.6036	0.5876	0.5775	0.5722	0.5706	0.5719	0.5754	0.5804	0.5865	0.5933	0.63279	0.67658	0.72257
12	0.6038	0.5872	0.5770	0.5719	0.5706	0.5721	0.5757	0.5808	0.5868	0.5935	0.63216	0.67658	0.72271
13	0.6044	0.5870	0.5766	0.5716	0.5704	0.5721	0.5758	0.5807	0.5867	0.5932	0.63153	0.67657	0.72258
14	0.6038	0.5859	0.5756	0.5709	0.5701	0.5721	0.5759	0.5810	0.5868	0.5932	0.63129	0.67671	0.72250
15	0.6038	0.5855	0.5753	0.5707	0.5702	0.5724	0.5762	0.5812	0.5870	0.5933	0.63150	0.67673	0.72225
16	0.6019	0.5837	0.5738	0.5698	0.5696	0.5720	0.5760	0.5811	0.5868	0.5932	0.63141	0.67676	0.72230
17	0.6011	0.5827	0.5731	0.5694	0.5696	0.5721	0.5762	0.5812	0.5869	0.5931	0.63141	0.67671	0.72230
18	0.6011	0.5826	0.5730	0.5695	0.5698	0.5724	0.5764	0.5813	0.5869	0.5931	0.63153	0.67668	0.72226
19	0.5995	0.5812	0.5721	0.5688	0.5694	0.5722	0.5762	0.5812	0.5868	0.5929	0.63157	0.67664	0.72228
20	0.5997	0.5815	0.5725	0.5695	0.5700	0.5726	0.5766	0.5814	0.5868	0.5930	0.63153	0.67659	0.72239
β (deg) / n	30	35	40	45	50	55	60	65	70	75	80	85	90
11	0.76640	0.80690	0.84469	0.87889	0.90911	0.93601	0.95943	0.97891	0.99483	1.00746	1.01642	1.02155	1.02369
12	0.76622	0.80697	0.84476	0.87866	0.90909	0.93614	0.95928	0.97883	0.99503	1.00745	1.01618	1.02170	1.02332
13	0.76599	0.80401	0.84465	0.87857	0.90921	0.93606	0.95921	0.97902	0.99498	1.00729	1.01637	1.02170	1.02360
14	0.76599	0.80704	0.84453	0.87866	0.90921	0.93599	0.95934	0.97892	0.99491	1.00750	1.01628	1.02164	1.02347
15	0.76600	0.80705	0.84458	0.87870	0.90917	0.93608	0.95929	0.97887	0.99499	1.00740	1.01627	1.02168	1.02343
16	0.76606	0.80698	0.84460	0.87869	0.90916	0.93908	0.95927	0.97892	0.99500	1.00738	1,01628	1.02165	1.02351
17	0.76607	0.80696	0.84460	0.87867	0.90918	0.93604	0.95927	0.97894	0.99496	1.00740	1.01624	1.02163	1.02348
18	0.76609	0.80694	0.84462	0.87868	0.90918	0.93604	0.95928	0.97891	0.99496	1.00740	1.01624	1.02164	1.02344
19	0.76609	0.80692	0.84461	0.87867	0.90918	0.93603	0.95928	0.97887	0.99497	1.00738	1.01624	1.02165	1.02339
20	0.76606	0.80693	0.84459	0.87866	0.90917	0.93604	0.95927	0.97888	0.99497	1.00738	1.01624	1.02162	1.02339

Table 5. Dimensionless stress intensity factors F_I along crack front ($\nu = 0$)

β (deg) / b/a	0	1	2	3	4	5	6	7	8	9	10	15	20	25
1.00	0.7689	0.7515	0.7384	0.7281	0.7197	0.7126	0.7065	0.7011	0.6963	0.6920	0.6881	0.6732	0.6632	0.6562
0.75	0.791	0.774	0.7546	0.7422	0.7323	0.7242	0.7174	0.7116	0.7065	0.7021	0.6983	0.6855	0.6798	0.6785
0.50	0.783	0.758	0.739	0.725	0.714	0.7054	0.6987	0.6933	0.6891	0.6858	0.6833	0.6798	0.6862	0.6983
0.25	0.678	0.748	0.628	0.614	0.606	0.6012	0.5992	0.5992	0.6008	0.6037	0.6077	0.6379	0.6764	0.7166

β (deg) / b/a	30	35	40	45	50	55	60	65	70	75	80	85	90
1.00	0.6510	0.6472	0.6442	0.6420	0.6402	0.6388	0.6377	0.6369	0.6363	0.6358	0.6355	0.6353	0.6352
0.75	0.6801	0.6837	0.6884	0.6939	0.6996	0.7053	0.7106	0.7155	0.7196	0.7230	0.7254	0.7269	0.7274
0.50	0.7135	0.7301	0.7471	0.7637	0.7793	0.7937	0.8065	0.8175	0.8267	0.8339	0.8390	0.8422	0.8433
0.25	0.7553	0.7919	0.8257	0.8563	0.8838	0.9081	0.9292	0.9470	0.9616	0.9728	0.9809	0.9858	0.9874

Table 6. Dimensionless stress intensity factors F_I along crack front ($\nu = 0.3$)

β (deg) / b/a	1	2	3	4	5	6	7	8	9	10	15	20	25
1.00	0.742	0.746	0.748	0.746	0.742	0.738	0.733	0.729	0.725	0.721	0.7078	0.6969	0.6889
0.75	0.740	0.742	0.743	0.741	0.739	0.735	0.732	0.728	0.725	0.722	0.7136	0.7091	0.7088
0.50	0.710	0.704	0.702	0.700	0.698	0.696	0.694	0.692	0.691	0.690	0.6936	0.7044	0.7200
0.25	0.601	0.583	0.573	0.570	0.570	0.572	0.576	0.581	0.587	0.593	0.6315	0.6797	0.7233

β (deg) / b/a	30	35	40	45	50	55	60	65	70	75	80	85	90
1.00	0.6821	0.6771	0.6729	0.6695	0.6667	0.6645	0.6627	0.6612	0.6601	0.6593	0.6587	0.6582	0.6585
0.75	0.7109	0.7148	0.7197	0.7253	0.7312	0.7370	0.7424	0.7473	0.7515	0.7549	0.7574	0.7592	0.7598
0.50	0.7382	0.7574	0.7767	0.7953	0.8128	0.8287	0.8429	0.8552	0.8653	0.8732	0.8788	0.8823	0.8835
0.25	0.7661	0.8069	0.8446	0.8787	0.9092	0.9360	0.9592	0.9789	0.9950	1.0074	1.0162	1.0216	1.0234

Table 7. Dimensionless stress intensity factors F_{I} along crack front $(b/a = 1)$

β (deg) / ν	0	1	2	3	4	5	6	7	8	9	10	15	20	25
0.00	0.7688	0.7515	0.7384	0.7281	0.7197	0.7126	0.7065	0.7011	0.6963	0.6920	0.6881	0.6732	0.6632	0.6562
0.30		0.742	0.746	0.748	0.746	0.742	0.738	0.733	0.729	0.725	0.721	0.7078	0.6969	0.6889
0.45		0.707	0.735	0.751	0.757	0.757	0.755	0.752	0.750	0.748	0.747	0.7381	0.7287	0.7222
0.50		0.689	0.728	0.751	0.760	0.762	0.761	0.760	0.759	0.758	0.756	0.7509	0.7427	0.7366

β (deg) / ν	30	35	40	45	50	55	60	65	70	75	80	85	90
0.00	0.6510	0.6472	0.6442	0.6420	0.6402	0.6388	0.6377	0.6369	0.6363	0.6358	0.6355	0.6353	0.6352
0.30	0.6821	0.6771	0.6729	0.6695	0.6667	0.6645	0.6627	0.6612	0.6601	0.6593	0.6587	0.6582	0.6585
0.45	0.7151	0.7099	0.7055	0.7017	0.6986	0.6960	0.6939	0.6922	0.6908	0.6898	0.6891	0.6883	0.6876
0.50	0.7300	0.7248	0.7204	0.7166	0.7134	0.7107	0.7085	0.7067	0.7053	0.7042	0.7035	0.7026	0.7020

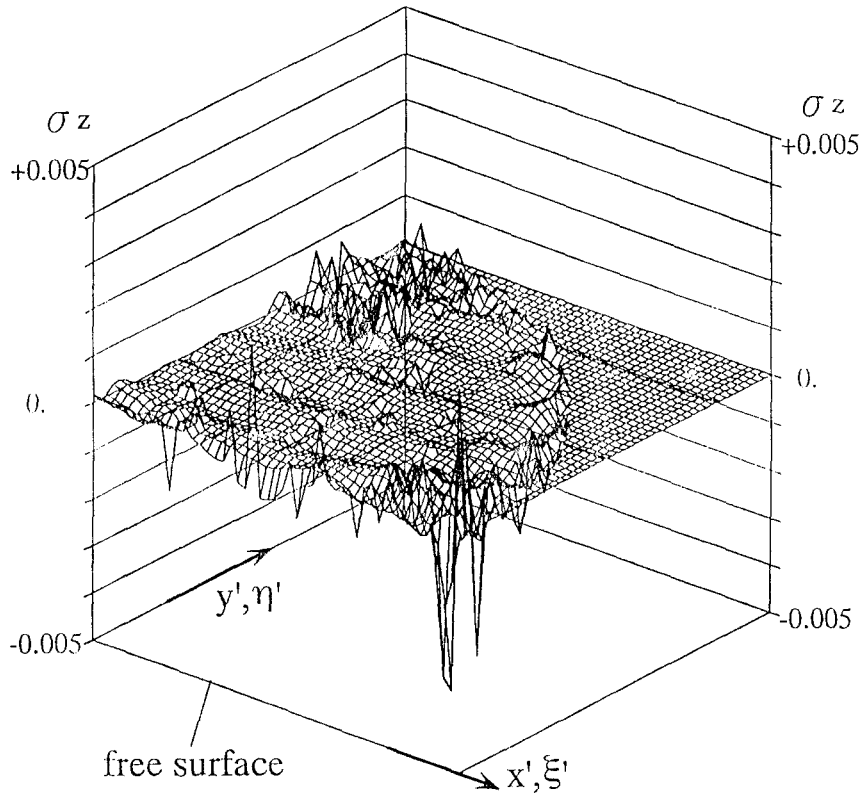

$$\sigma_z = \frac{b}{2\pi\Phi}\sum_{i=0}^{l}\alpha_i\left(A_i + B_i\right) + 1$$

Figure 13. Compliance of boundary condition ($n = 18, \nu = 0.3, b/a = 1$).

Table 8. Magnitude and position of maximum stress intensity factors $F_{\mathrm{I}\max}$ and the accuracy of Murakami's formula ($\nu = 0.3$)

b/a ($a = 1.0$)	$F_{\mathrm{I}\max}$	β (deg)	$F_{\mathrm{I}\max *}$	δ (%)
1.00	0.748	3	0.668	+2.7
0.75	0.7598	90	0.6316	−2.9
0.50	0.8835	90	0.6636	+2.0
0.25	1.0234	90	0.6464	−0.6

Tables 1–4 show the convergency of dimensionless stress intensity factors along the crack front with increasing parameter n. For $\nu = 0.3$ the present results have the convergency in the 4 significant digits for most cases when $n = 19$ and in the 3 significant digits for worst cases in the range $\beta = 0 \sim 10$ degree.

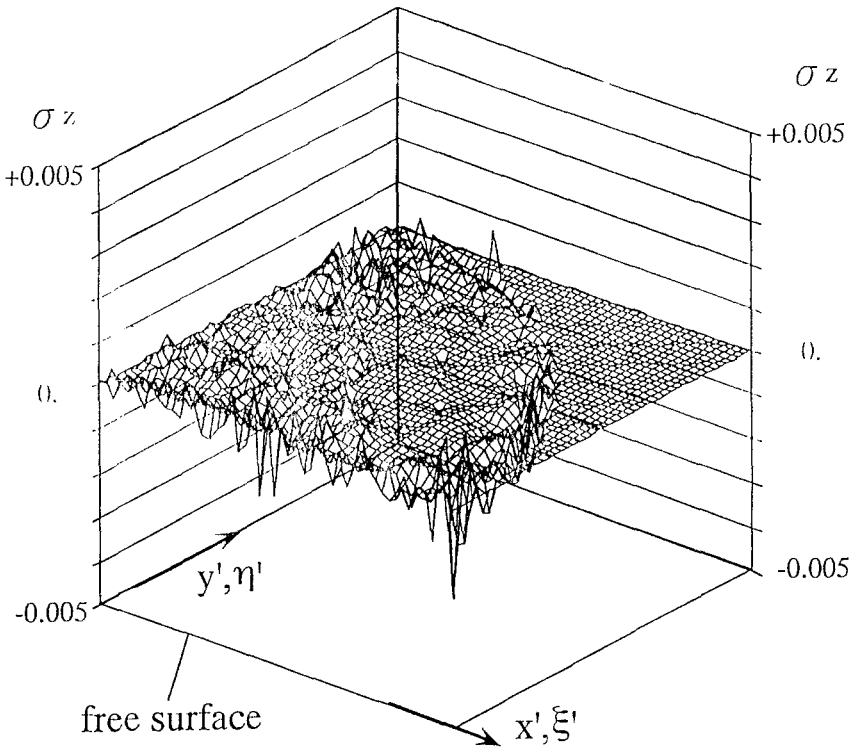

$$\sigma_z = \frac{b}{2\pi\Phi}\sum_{i=0}^{l}\alpha_i\left(A_i + B_i\right) + 1$$

Figure 14. Compliance of boundary condition ($n = 18, \nu = 0.3, b/a = 0.25$).

Table 9. Crack opening displacement $M_{\mathrm{I}}(0,0)$

b/a / ν	0.00	0.25	0.50	0.75	1.00
0.00	1.4543	1.3439	1.2528	1.1944	1.1555
0.30	1.4543	1.4201	1.3815	1.3504	1.3266
0.45	1.4543				1.5045
0.50	1.4543				1.5863

4.3. VARIATION OF STRESS INTENSITY FACTOR AND CRACK OPENING DISPLACEMENT

Tables 5–7 and Figures 17–19 show the variation of dimensionless stress intensity factors F_{I} along the crack front. When Poisson's ratio ν is not zero, it is well known that the stress intensity factor has the peak value close to the free surface except for the small value of b/a. For $b/a = 1$ and $\nu = 0.3$ maximum value $F_{\mathrm{I}\max} = 0.748$ occurs at $\beta = 3$ degree. Figure 20 shows the variation of dimensionless stress intensity factors $M_{\mathrm{I}}(\beta)$ along the crack front in

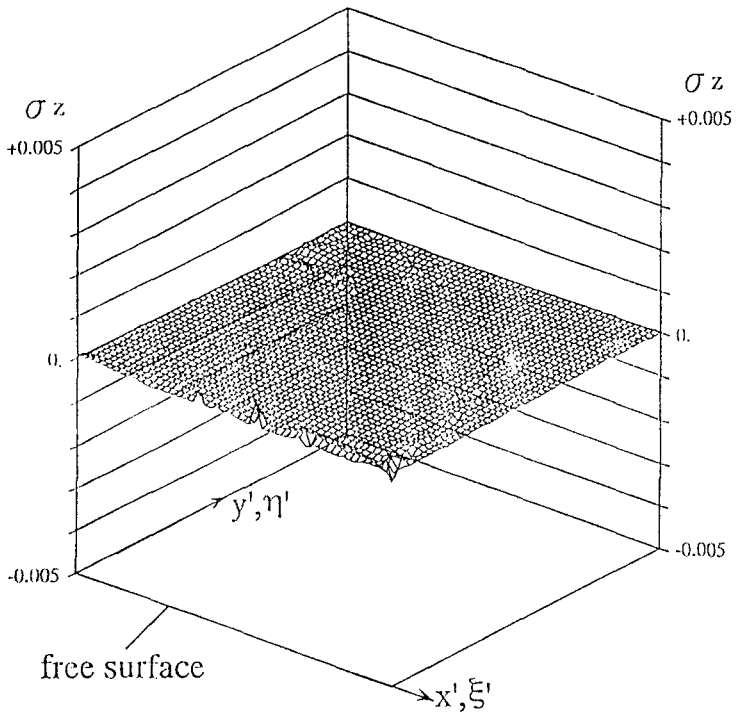

$$\sigma_z = \frac{b}{2\pi\mathfrak{p}} \sum_{i=0}^{l} \alpha_i (A_i + B_i) + 1$$

Figure 15. Compliance of boundary condition ($n = 18, \nu = 0, b/a = 1$).

comparison with Isida [17, 19], Raju–Newmann [9, 10] and Yagawa et al. [7]. Isida's result is in close agreement with the present result except near the free surface.

In Table 8 the accuracy of Murakami's formula (16) for arbitrary shaped crack using root of crack area [29] is shown. In this table Murakami's formula gives approximate maximum values of stress intensity factor of a semi-elliptical crack within 3 percent error.

$$\left.\begin{aligned} &K_{\mathrm{I}\max} = 0.650 \times \sigma_z \sqrt{\pi \sqrt{\text{area}}}, \\ &\text{where} \\ &\text{area} = \pi ab/2 \end{aligned}\right\}. \tag{16}$$

Figures 21–26 indicate variation of dimensionless crack opening displacement $M_{\mathrm{I}}(x', y')$. Figure 27 shows crack opening displacement of semi-elliptical surface crack on the free surface $U_z(x', 0)$ in comparison with an elliptical crack. In Table 9 the values of $M_{\mathrm{I}}(0, 0)$ are tabulated for various aspect ratio and Poisson's ratio. One of the authors has carried out the research of crack identification from the data of strain measured around the crack [30, 31]. From Table 9 it seems possible to estimate the depth of a surface crack by measuring the surface displacement of the crack.

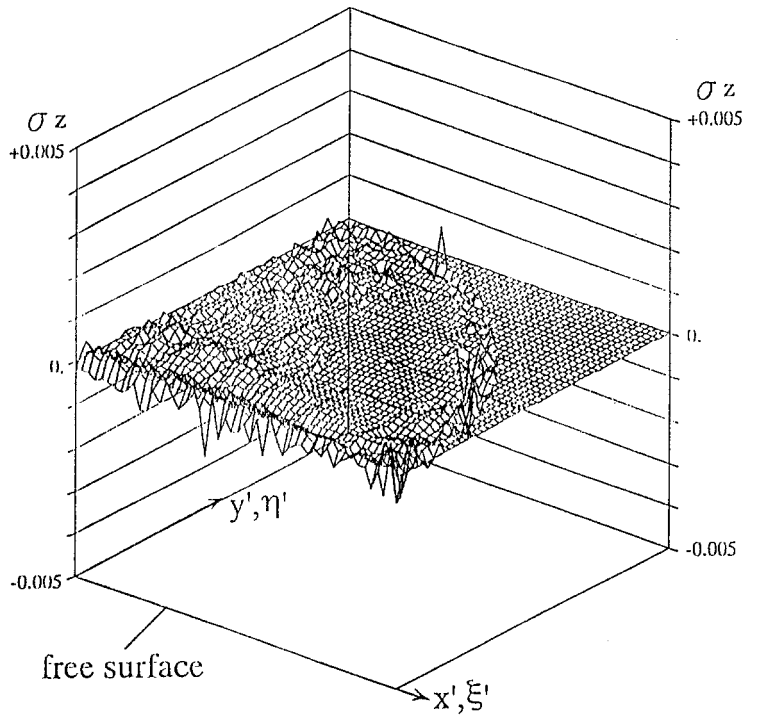

$$\sigma_z = \frac{b}{2\pi\Phi}\sum_{i=0}^{l}\alpha_i\left(A_i + B_i\right) + 1$$

Figure 16. Compliance of boundary condition ($n = 18, \nu = 0, b/a = 0.25$).

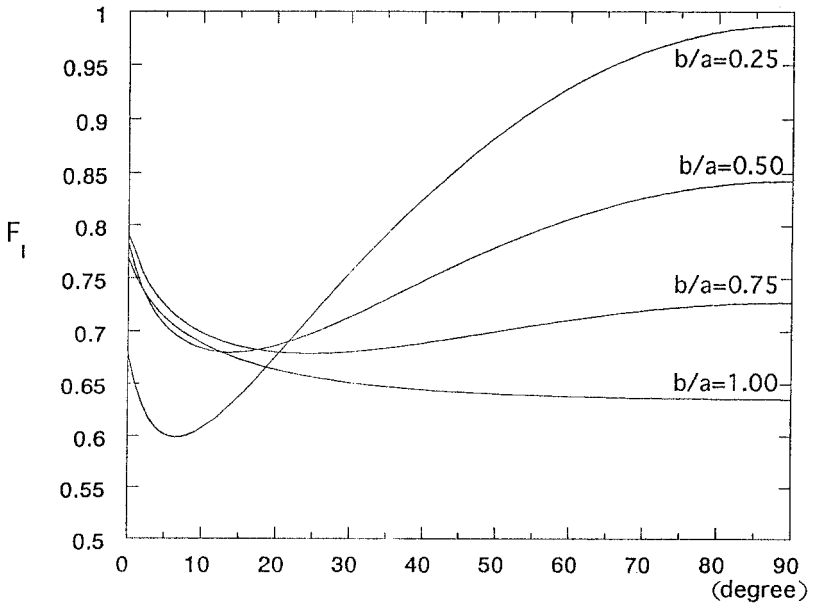

Figure 17. Variation of dimensionless stress intensity factors F_{I} along crack front ($\nu = 0$).

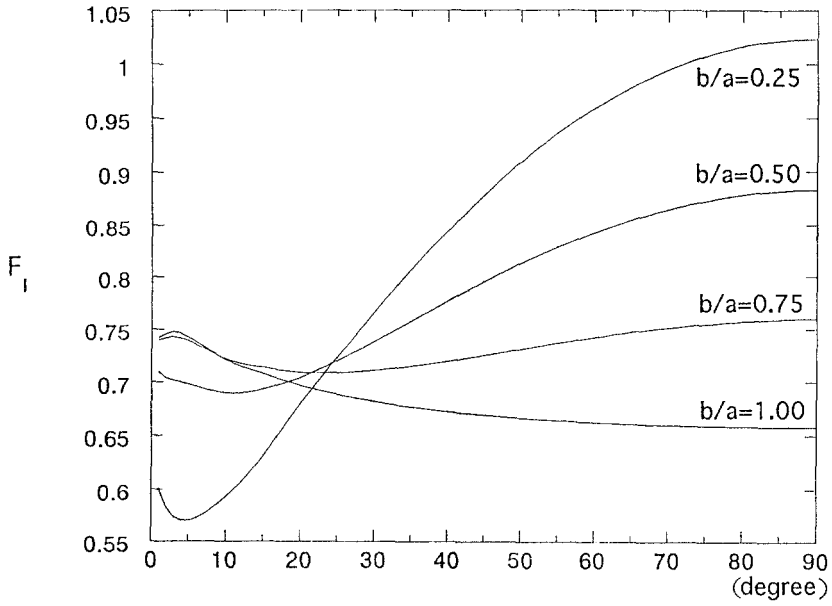

Figure 18. Variation of dimensionless stress intensity factors F_{I} along crack front ($\nu = 0.3$).

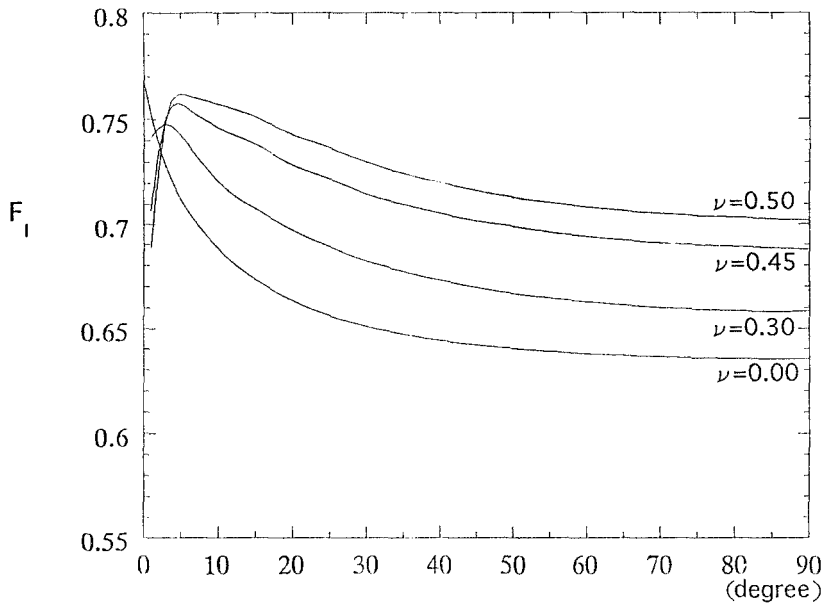

Figure 19. Variation of dimensionless stress intensity factors F_{I} along crack front ($b/a = 1$).

5. Conclusion

In this paper, a singular integral equation method useful for 3D crack problems is discussed. The conclusions are summarized as follows:

(1) The 3D crack problems were formulated in terms of singular integral equations with singularity of the form r^{-3} on the basis of the body force method, where the Green's function for a force doublet was used as the fundamental solution. The unknown function of

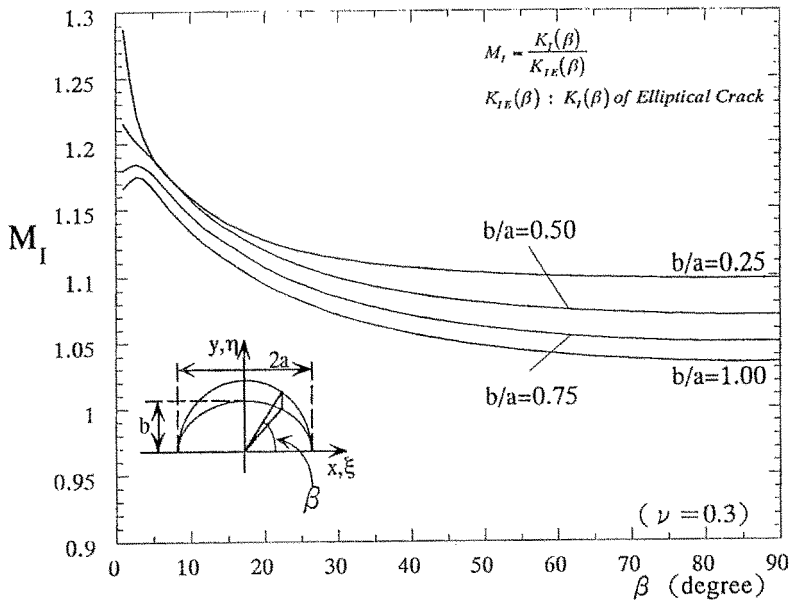

Figure 20. Variation of dimensionless stress intensity factors M_{I} along crack front in comparison with previous results ($\nu = 0.3$).

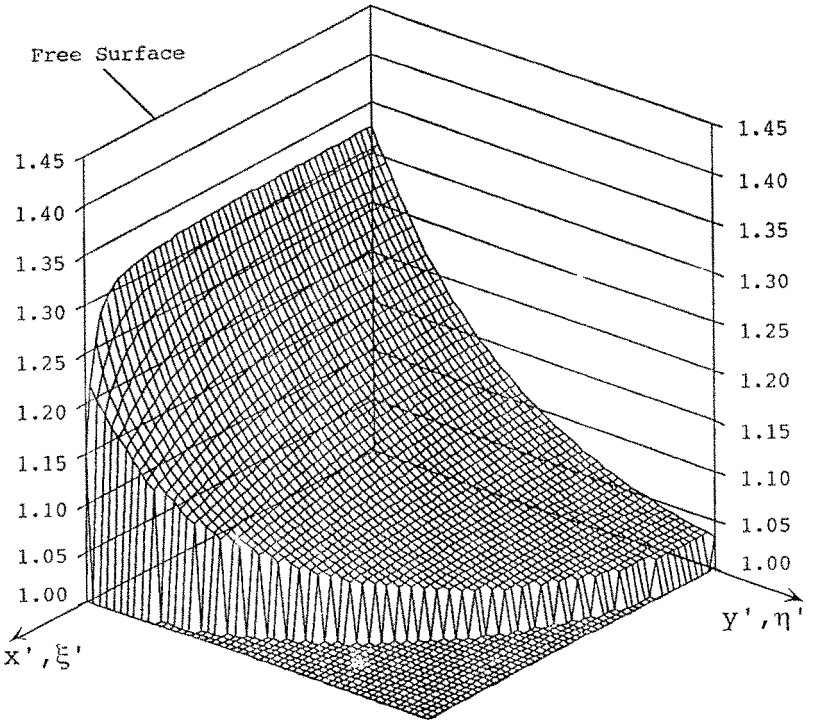

Figure 21. Variation of crack opening displacement $M_{\mathrm{I}}(x', y')$ along crack surface ($n = 18, \nu = 0.3, b/a = 1$).

the body force density was approximated by the product of a fundamental density function and a weight function. Hypersingular integrals were evaluated exactly; then, the integral for embedded elliptical crack can be calculated within the error of 1×10^{-10} in most cases.

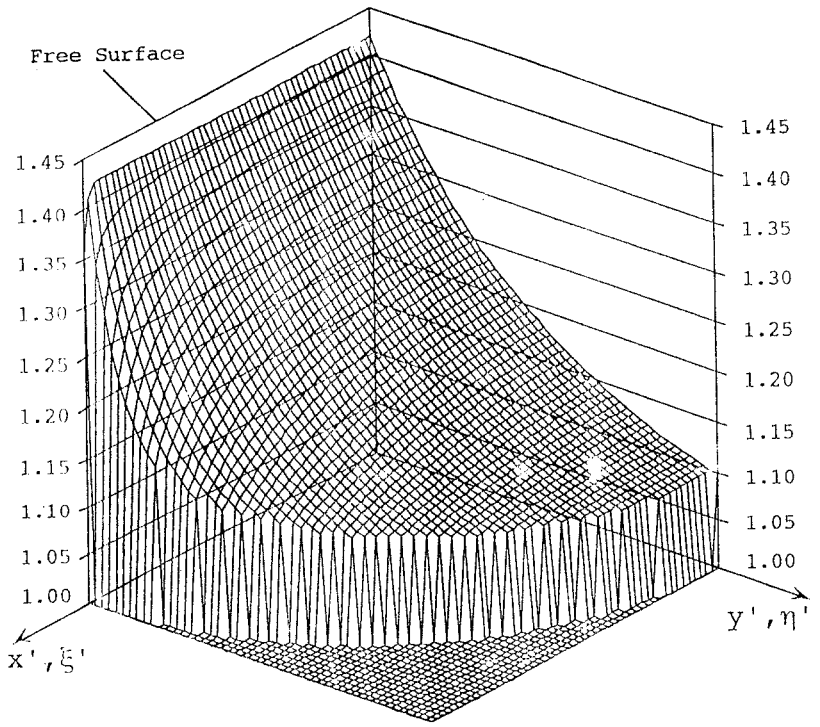

Figure 22. Variation of crack opening displacement $M_I(x', y')$ along crack surface $(n = 18, \nu = 0.3, b/a = 0.25)$.

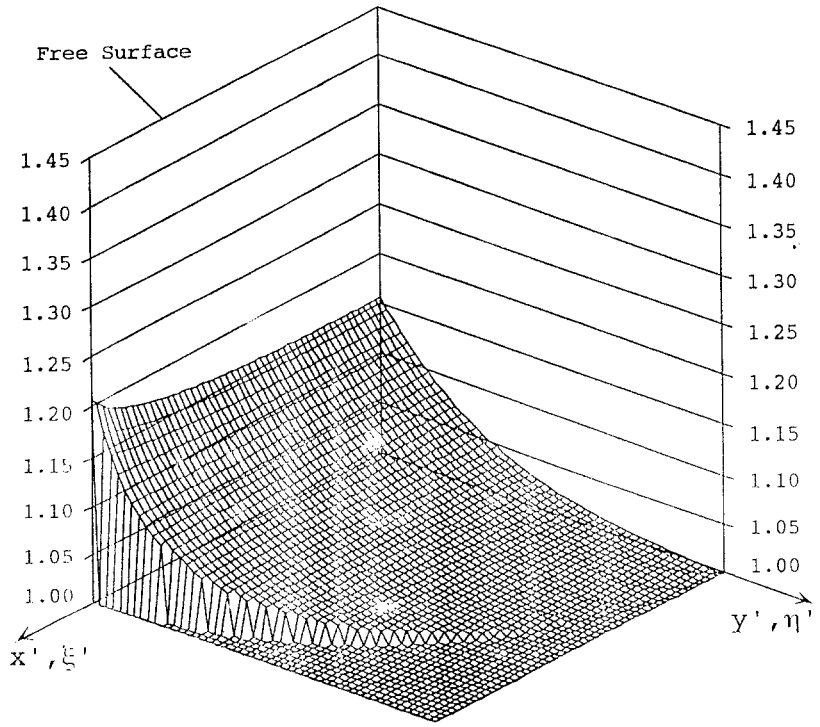

Figure 23. Variation of crack opening displacement $M_I(x', y')$ along crack surface $(n = 18, \nu = 0, b/a = 1)$.

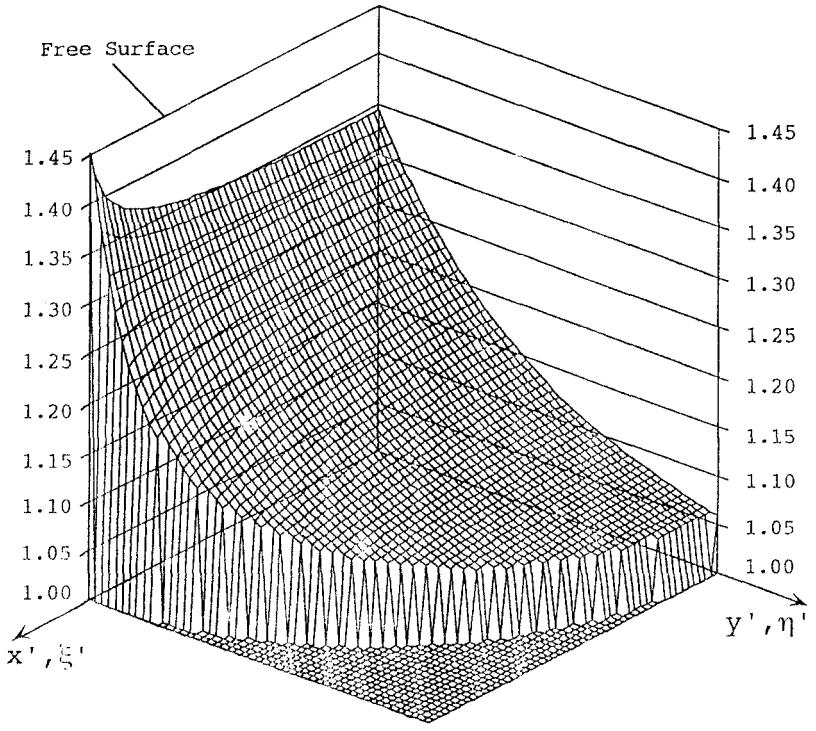

Figure 24. Variation of crack opening displacement $M_I(x', y')$ along crack surface ($n = 18, \nu = 0, b/a = 0.25$).

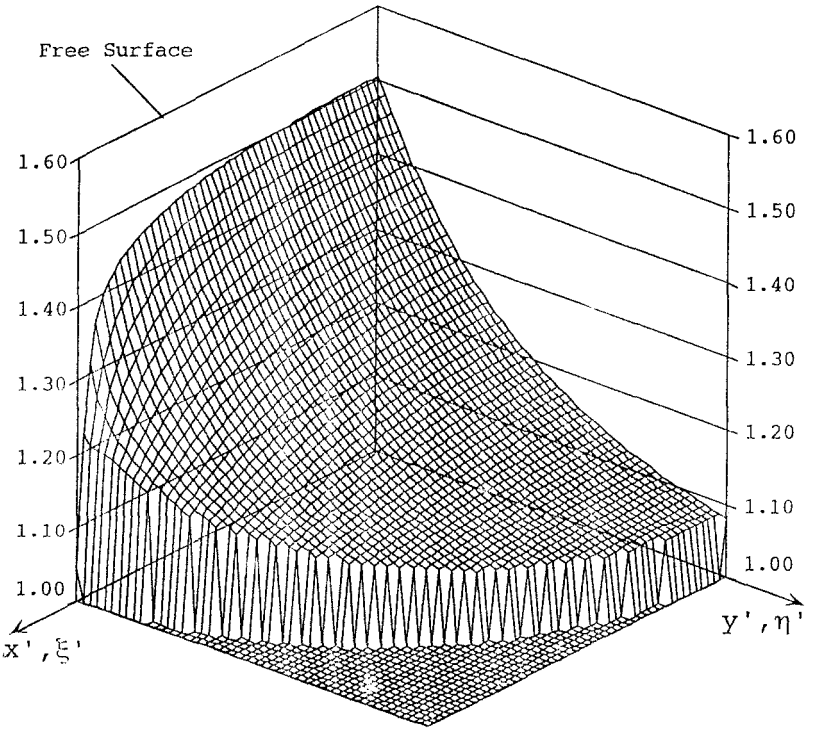

Figure 25. Variation of crack opening displacement $M_I(x', y')$ along crack surface ($n = 25, \nu = 0.45, b/a = 1.00$).

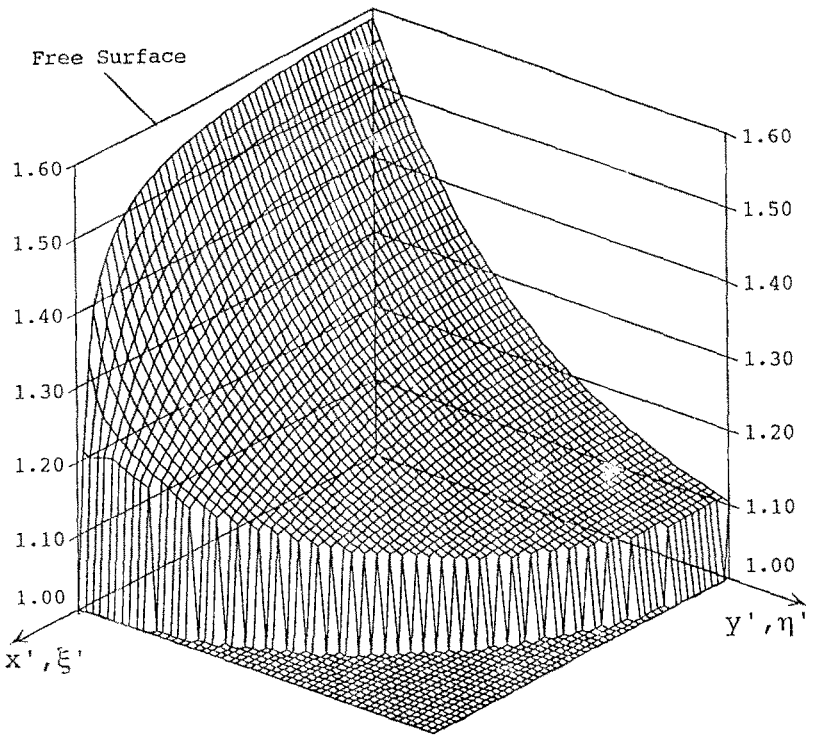

Figure 26. Variation of crack opening displacement $M_I(x', y')$ along crack surface $(n = 25, \nu = 0.5, b/a = 1.00)$.

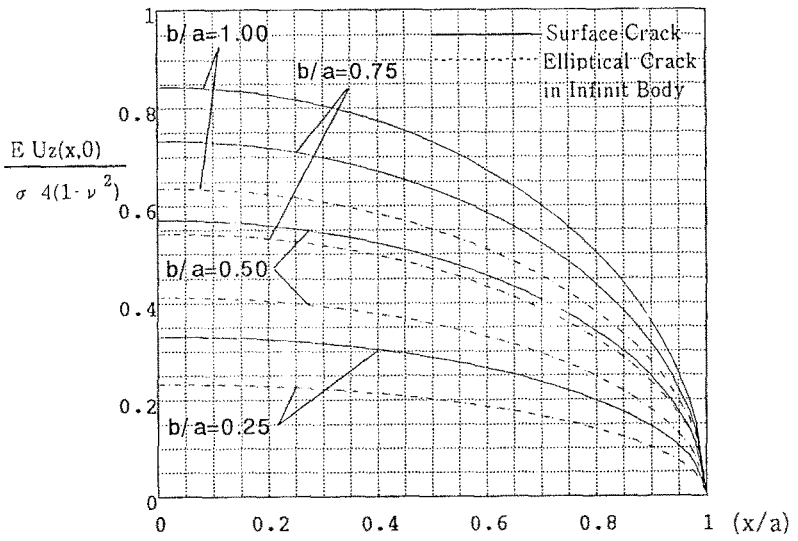

Figure 27. Crack opening displacement $U_z(x, 0)$ on the free surface in comparison with an elliptical crack.

(2) The present method gives rapidly converging numerical results; then the smooth variations of stress intensity factor along the crack front and crack opening displacement along the crack surface were obtained. The boundary condition was found to be satisfied within the error of 3×10^{-3} throughout the crack surface.

(3) The variations of stress intensity factor of semi-elliptical crack and crack opening displacement were tabulated or charted for the aspect ratio and Poisson's ratio. For semi-circular crack, it was found that the maximum stress intensity factor appears near the free surface with the eccentric angle $\phi = 3$ degree. It was found that the maximum stress intensity factor of semi-elliptical crack can be evaluated by using Murakami's approximate formula within the 3 percent error.

References

1. H. Miyamoto and T. Miyoshu, *Proceedings of Symposium on High Speed Computing of Elastic Structures*, IUTAM (1970) 137–155.
2. D.M. Tracy, *Nuclear Engineering and Design* 26 (1974) 282–290.
3. T.K. Hellen and W.S. Blackburn, *Computational Fracture Mechanics*, ASME (1975) 103.
4. H. Miyata and K. Kusumoto, *Transactions of JSME* 43–367 (1977) 816–824.
5. H. Miyamoto and K. Kashuma, *Transactions of JSME* 43–370 (1977) 816–824.
6. Y. Murakami and Y. Okazaki, *Transactions of JSME* 43–376 (1977) 4397–4408.
7. G. Yagawa, M. Ichimiya and Y. Ando, *Proceedings of the 1st International Conference on Numerical Methods in Fracture Mechanics*, Swansea (1978) 249–267.
8. T. Nishioka, G. Yagawa, and N. Ogura, *Transactions of JSME* 45–395 (1979) 717–725.
9. I.S. Raju and J.C. Newmann, *Engineering Fracture Mechanics*, 11 (1979) 817–829.
10. J. C. Newmann and I.S. Raju, *Analysis of Surface Cracks in Finite Plates under Tension and Bending Loads* NASA TP-1578 (1979).
11. H. Nisitani and Y. Murakami, *International Journal of Fracture* 10 (1974) 353–368.
12. J. Weaver, *International Journal of Solids and Structures* 13–4 (1979) 321–330.
13. K. Hayashi and H. Abe, *Transactions of JSME* 46–408 (1980) 886–893.
14. H. Takakuda, T. Koizumi and T. Shibuya, *Transactions of JSME* 50–454 (1984) 1184–1192.
15. Y. Murakami and M. Isida, *Transactions of JSME* 50–455 (1984) 1359–1366.
16. M. Isida, H. Noguchi and T. Yoshida, *International Journal of Fracture* 26 (1984) 157–188.
17. M. Isida and H. Noguchi, *Engineering Fracture Mechanics* 20–3 (1984) 387–408.
18. M. Isida, H. Tsuru and H. Noguchi, *Transactions of JSME* 59–561 (1993) 1270–1278.
19. H. Noguchi, M. Isida and T. Tsuru, *Transactions of JSME* 59–561 (1993) 1279–1286.
20. N.A. Noda and K. Oda, *International Journal of Fracture* 58 (1992) 285–304.
21. N.A. Noda, K. Oda and T. Matsuo, *Localized Damage II, Vol. 2: Computational Methods in Fracture Mechanics*, M.H. Adiabadi, H. Nisitani and D.J. Cartwright (eds.), Computational Mechanics Publications, Southampton (1992) 35–56.
22. N.A. Noda and T. Matsuo, *Transactions of the Japan Society of Mechanical Engineers* 58–555 A (1992) 2179–2184.
23. N.A. Noda and T. Matsuo, *Transactions of the Japan Society of Mechanical Engineers* 55–559 A (1993) 785–791.
24. N.A. Noda and T. Matsuo, *Fracture Mechanics; 25th Volume, ASTM STP 1220*, F. Erdogan and R.J. Hartranft (eds.), submitted.
25. N.A. Noda and T. Matsuo, *International Journal of Fracture* 70 (1995) 147–165.
26. H. Nisitani, *Journal of the Japan Society of Mechanical Engineers* 70 (1967) 627–632. *Bulletin of Japan Society of Mechanical Engineers* 11 (1968) 14–23.
27. H. Nisitani, *Body Force Method of Notched Problem*, G.C. Sih (ed.), Leyden (1974) 1–68.
28. H. Nisitani and D.H. Chen, *The Body Force Method (Taisekiryokuho in Japanese)*, Baifukan, Tokyo (1987) 89–90.
29. J. Hadamard, *Lectures on Cauchy's Problem in Linear Partial Differential Equations* (1923) Yale University Press.
30. D.H. Chen, N.A. Noda, K. Oda and S. Harada, *Localized Damage II, Vol. 2: Computational Methods in Fracture Mechanics*, M.H. Adiabadi, H. Nisitani, and D.J. Cartwright (eds.), Computational Mechanics Publications, Southampton (1992) 57–75.
31. D.H. Chen, N.A. Noda, K. Oda and S. Harada, *International Journal of Fracture* 72 (1995) 343–358.